CORRELATION OF THE LYNX-XZ170 FLIGHT-TEST RESULTS UP TO AND BEYOND THE STALL BOUNDARY

Benton H. Lau
Aerospace Engineer
NASA Ames Research Center
Moffett Field, California

Alexander W. Louie
Engineer
Sterling Software
Palo Alto, California

Costantinos P. Sotiriou
Principal Engineer in Dynamics
and
Nicholas Griffiths
Principal Engineer in Aerodynamics
Westland Helicopters Limited
Yeovil, Somerset
United Kingdom

Abstract

Results from two rotorcraft codes were correlated with flight-test data obtained from the Lynx-XZ170 helicopter. The Lynx XZ170 features a hingeless rotor system with four blades having rectangular tip planforms. The flight-test data base includes steady, level flight conditions at different thrust levels and advance ratios up to and beyond the rotor stall boundary. Rotor performance, control inputs, blade and control loads were compared with results from the Comprehensive Analytical Model of Rotorcraft Aerodynamics and Dynamics developed by Johnson Aeronautics (CAMRAD/JA) and the R150 rotor analysis developed by Westland Helicopters Limited (WHL) and the Defense Research Agency. Effects on blade loads correlation are examined by varying CAMRAD/JA modeling parameters such as lag-damper model, stall model, and wake model. In addition, effects of rotor trim condition on blade structural loads and methods of calculating the loads are investigated. The influence of the fuselage on rotor loads is presented using the R150 analysis. CAMRAD/JA calculations for the flatwise bending moments at the outboard stations compare reasonably well with the flight-test data. Near the hub, CAMRAD/JA flatwise moment calculations compare well with the data at low speeds but fairly at high speeds. R150 correlations of the flatwise bending moments are very good near the hub and at the outboard station, but only fair at the inboard station. For the edgewise bending moments, both the CAMRAD/JA and R150 comparisons with data are good near the hub and fair at the outboard stations. Except for a phase difference, the CAMRAD/JA correlation of the lag-damper load is reasonably good using the nonlinear lag-damper model. Although the general trends of the vibratory pitch-link load data are captured by both analytical codes, the details of the waveform are not.

Presented at the American Helicopter Society 49th Annual Forum, St. Louis, Missouri, May 19–21, 1993.

Notation

A	Main-rotor disk area, $A = \pi R^2$, ft^2
b	Number of blades
c	Blade chord, ft
C_{pp}	Pitch-link load coefficient, $C_{pp} = \frac{eP_{LL}}{1/2\ \rho c^2 R(\Omega R)^2}$
C_W	Aircraft-weight coefficient, $C_W = W/\rho\ A(\Omega R)^2$
C_W/σ	Ratio of aircraft-weight coefficient to rotor solidity
e	Pitch-horn length, ft
M_X, M_Z	Vibratory flatwise and edgewise bending moments, respectively, ft-lb (positive for blade flapping up and lagging back)
n	Ratio of the main-rotor RPM to nominal RPM
P_{LL}	Half peak-to-peak magnitude of the vibratory pitch-link load, lb
$P/\rho_o n^3$	Normalized main-rotor power, hp
R	Rotor radius, ft
r	Blade radial station, ft
V	True air speed, kt
W	Aircraft weight, lb
α	Blade section angle of attack, deg

Figure 1. Lynx-XZ170 helicopter.

μ	Advance ratio, $\mu = V/\Omega R$
Ω	Main-rotor rotational speed, rad/s
ρ	Air density, slug/ft^3
ρ_0	Nondimensional air density , $\rho_0=\rho/$(ISA density)
σ	Rotor solidity, $\sigma=$ bcR/A

Introduction

Understanding the complex aeroelastic behavior of a helicopter remains a challenging task to rotorcraft analysts. The rotor aerodynamics, the rotor-wake fuselage interaction, the retreating blade stall, and the structural dynamics have to be included in an analytical model to accurately predict the rotor performance and loads. The calculated results must be correlated with experimental data, preferably with data from flight tests or full-scale wind-tunnel tests, to substantiate the accuracy of the analysis. Although a number of helicopter flight tests and full-scale wind-tunnel tests are documented in the literature, the majority apply to articulated rotors (Refs. 1-5). Limited data from full-scale, soft-inplane hingeless rotors are available to the public (Refs. 6-8).

NASA Ames Research Center and Westland Helicopters Limited (WHL) established a joint research program to document the flight tests of a hingeless Lynx helicopter and perform a correlation study with these data. The flight tests were conducted by WHL in 1985 to evaluate the performance and load characteristics of the Lynx-XZ170 helicopter equipped with rectangular metal blades. The helicopter was tested up to and beyond the retreating-blade stall boundary (defined by a limit of the vibratory pitch-link load). Test data consist of 27 steady, level flight conditions at different thrust levels and advance ratios. Rotor structural loads, performance, and flight conditions are documented in Ref. 9.

An additional objective of the joint research program was to examine the ability of both the Comprehensive Analytical Model of Rotorcraft Aerodynamics and Dynamics developed by Johnson Aeronautics (CAMRAD/JA) (Ref. 10) and the R150 rotor analysis developed by WHL and the Defense Research Agency (DRA, formerly the Royal Aerospace Establishment), to correlate rotor performance, control settings, and blade and control loads with flight data up to and beyond the stall boundary. Out of the 27 flight conditions, 11 were selected for performance correlation and four for loads correlation.

This paper provides a general description of the Lynx-XZ170 helicopter, the flight test, the R150 and CAMRAD/JA analyses, the assumptions and approximations in modeling the aircraft and the rotor, and the calculated results compared with flight data. Recommendations for improving the correlation are also discussed.

Flight-Test Description

Lynx-XZ170 Helicopter

Figure 1 shows a photograph of the Lynx-XZ170 helicopter, and Fig. 2 is a three-view drawing that summarizes the basic aircraft dimensions. The Lynx

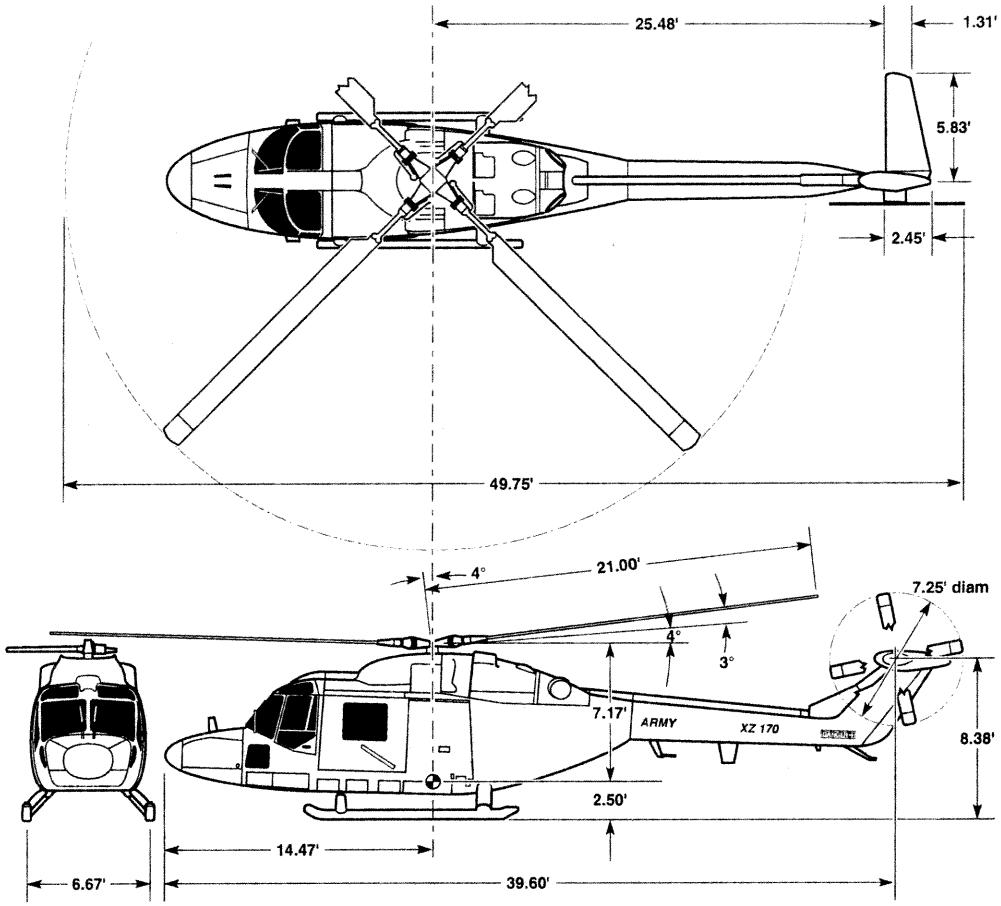

Figure 2. Three-view drawing of the Lynx-XZ170 helicopter.

XZ170 is a utility helicopter powered by two 800-horsepower engines through a three-pinion gearbox. The main rotor features a hingeless hub, presented in Fig. 3, with a hydraulic lag damper (not shown). The blade is rectangular in planform and is constructed from three airfoil sections: NPL9618 at r/R=0.286, NPL9615 at r/R=0.85, and NPL9617 at the tip (see Fig. 4). The general characteristics of the main rotor are summarized in Table 1. The tail rotor has an articulated hub with four blades having the NPL9615 airfoil section.

Instrumentation and Data Reduction

The flight measurements consisted of hub, blade, and aircraft parameters. The hub parameters included main-rotor shaft torque, blade feathering angle, pitch-link load, lag-damper load, collective control load, cyclic control loads, and three pairs of flatwise and edgewise bending moments on the rotor hub. The blade parameters included

Table 1. General characteristics of the Lynx XZ170 main rotor.

Number of blades	4
Nominal tip speed	700 ft/s
Rotor radius	21 ft
Rotor solidity	0.07858
Blade mass	6.21 slug
Airfoil sectional profile	
at r/R=0.286	NPL9618
at r/R=0.85	NPL9615
at r/R=1.0	NPL9617
Linear twist slope	–8°
Hydraulic lead-lag damper	

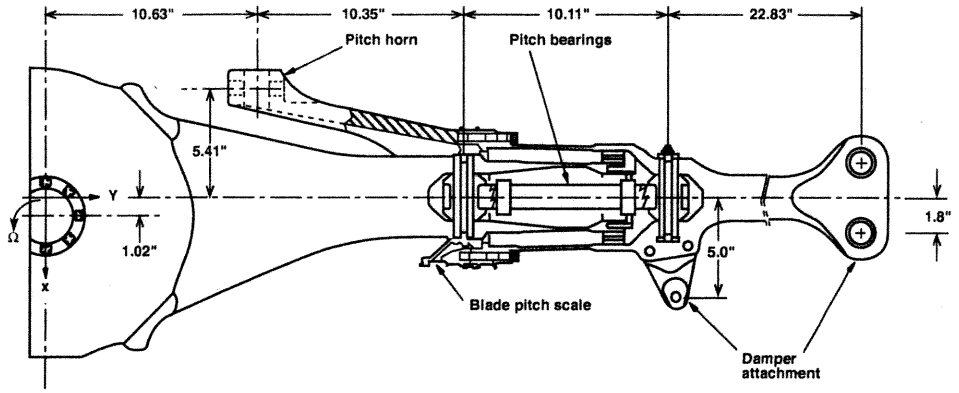

Figure 3. Hub assembly of the main-rotor system.

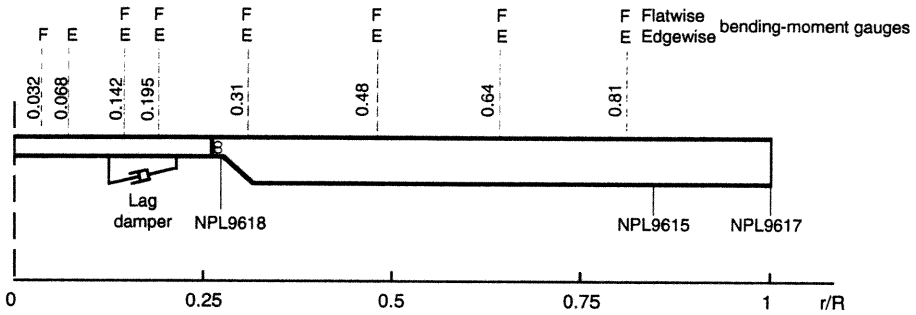

Figure 4. Locations of flatwise and edgewise bending-moment gauges, airfoil sections, and lag damper.

pairs of flatwise and edgewise bending moments at four radial stations. Figure 4 shows the locations of these seven pairs of bending-moment gauges, the blade sectional profiles, and the lag damper. The aircraft parameters included pressure altitude, outside air temperature, indicated airspeed, main-rotor rotational speed, aircraft weight, total engine power, aircraft rate of climb, and aircraft pitch and roll attitudes.

All measurements were simultaneously digitized and recorded by the Multiplex On-board Data Acquisition System (MODAS) for approximately 20 seconds. The aircraft parameters were sampled at 70.62 Hz providing about 1412 data points and the averaged values were obtained from a strip-chart recorder. The hub and blade parameters were sampled at 1129.93 Hz over 106 revolutions providing approximately 22600 data points or 213 samples/revolution. Although MODAS recorded over 100 revolutions of data, the data were averaged using only the middle 80 revolutions. Next, the Fourier coefficients were calculated for the first 20 harmonics. The mean values of all bending moments and pitch-link loads, however, are suspect because of difficulties encountered during calibration. Hence, only the vibratory bending moments and loads are used in the correlation study.

Flight Conditions

All data were obtained under steady, level flight conditions. The flight tests were grouped into five major flights according to the aircraft load. Figure 5 summarizes the flight conditions in terms of C_W/σ as a function of advance ratio. Flights 487 and 499 were flown under the low-load conditions at C_W/σ=0.07 and 0.08, respectively; Flight 497 was flown under the mid-load condition at C_W/σ=0.095; and Flights 503 and 504 were flown under the high-load conditions at C_W/σ=0.11 and 0.12, respectively. As the aircraft approached the retreating-blade stall boundary, a steep rise in the vibratory pitch-link load occurred as shown in Fig. 6. The stall boundary in Figs. 5 and 6 is defined by a limit of pitch-link load coefficient C_{pp}=0.013. Waveforms of the pitch-link load from Flight 503 are shown in Fig. 7, which clearly illustrates the blade stall characteristics on the retreating side of the rotor.

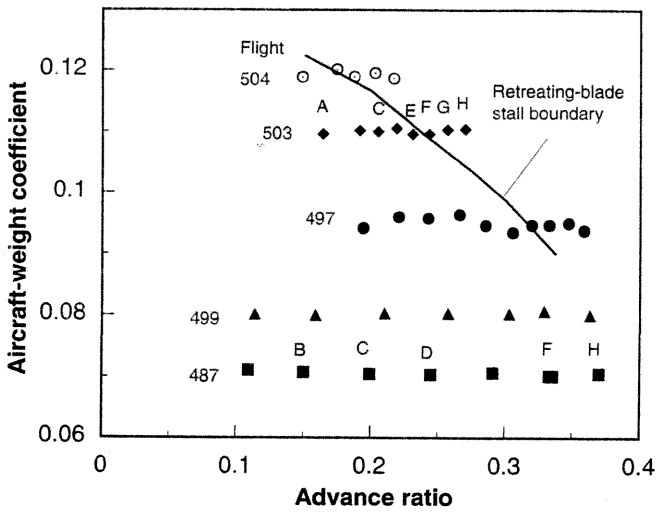

Figure 5. Summary of all flight-test conditions.

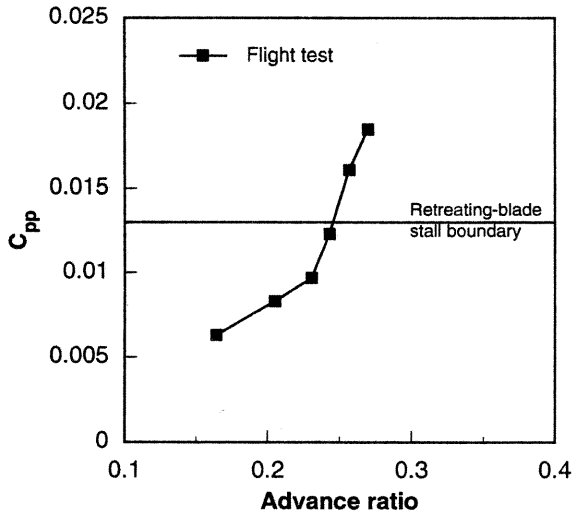

Figure 6. Pitch-link load coefficient and retreating-blade stall boundary for Flight 503.

Description of Analyses

R150 Analysis

The R150 rotor-analysis code developed by WHL and DRA calculates the rotor performance and structural loads for steady flight conditions. The structural-dynamic model in R150 utilizes a consistent derivation of the nonlinear coupled flap-lag-torsion behavior of a twisted, non-uniform blade. The code is capable of modeling multiple load paths and blades with a non-straight elastic axis. A "unified formulation" method developed by Hansford in Ref. 11 was incorporated in the analysis to accommodate the higher mode contributions to the applied spanwise loadings, which are normally neglected because of the limitation of a finite number of mode shapes. This method is especially applicable to modeling concentrated loads such as those generated by a lag damper.

The aerodynamic model consists of a lifting-line theory for a multiple airfoil-section blade with a simple representation of the yawed flow effect on dynamic stall (Ref. 12). The unsteady aerodynamics are represented by an indicial model incorporating a time-delay method for dynamic stall as described in Refs. 13 and 14.

The wake model calculation includes the effects of flow over the fuselage using a slender-body theory. A series of modified vortex rings is then positioned and adjusted to model the local vortex effects. The near-wake model is modified to relate the vortex strength to local blade loading for correlation improvement of the flatwise bending moment (Ref. 15).

For the specific correlation of rotor loads, the pitch and roll moments at the rotor hub, calculated from flight-test data by a modal analysis program (Ref. 16), were specified for each rotor trim condition. With specified aircraft weight, blade flapping, and estimated fuselage lift and drag, an iterative procedure was applied to trim the rotor in the longitudinal direction (Ref. 17).

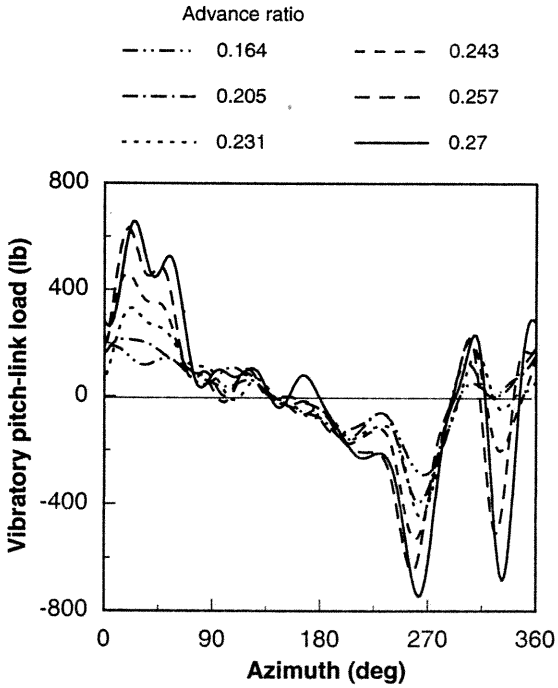

Figure 7. Measured vibratory pitch-link loads from Flight 503.

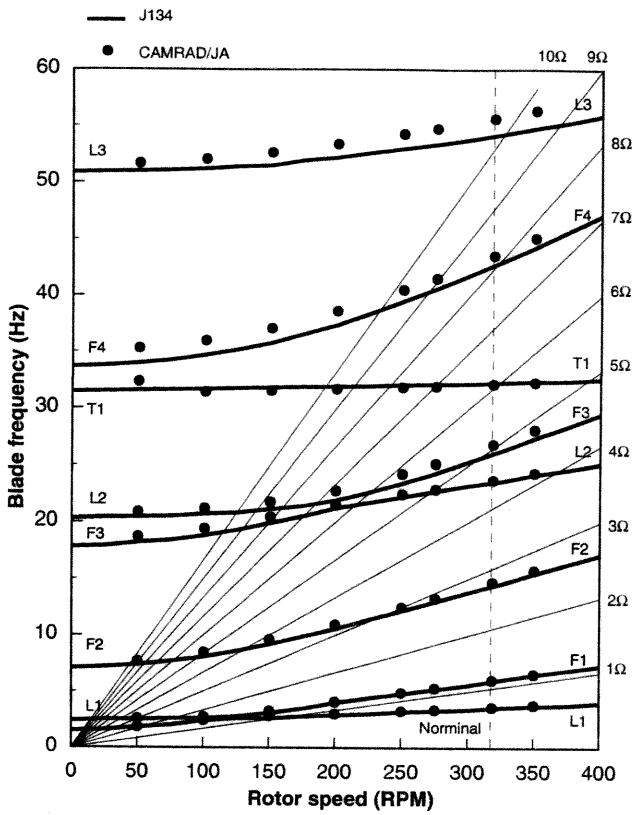

Figure 8. Natural frequencies (in vacuo) of the main-rotor blade calculated using J134 and CAMRAD/JA.

Eight coupled modes (four flap, three lag, and one torsion) were specified to model the rotor blade, and the calculated results were reconstructed using 12 harmonics (Ref. 18).

CAMRAD/JA Analysis

CAMRAD/JA is a comprehensive analytical model designed to calculate rotor performance, structural loads, aircraft vibration and gust response, flight dynamics and handling qualities, and system aeroelastic stability. The analytical development of CAMRAD/JA is discussed in Ref. 10.

For performance and control-input correlations, the Lynx helicopter was modeled in CAMRAD/JA with main and tail rotors. CAMRAD/JA calculated the trim solution for a specified flight speed, aircraft weight, and atmospheric conditions. The trim iteration computed the rotor controls and the aircraft pitch and roll angles to balance the force and moment on the aircraft. As a result, CAMRAD/JA overestimated the first harmonic of the hub moment. Subsequently, for the rotor loads correlation, the Lynx helicopter was modeled as a single main rotor. The trim solution was calculated for a specified propulsive force, aircraft lift, and cyclic flap angles. Both the propulsive force and aircraft lift were specified using the free-flight solution values; the cyclic flap angles were then adjusted until the flatwise bending moment near the hub matched with flight data. Effects of both the free-flight and hub-moment trim solutions on blade loads are presented in the section on rotor loads correlation.

The blade loads were calculated using 12 harmonics and included six coupled flap and lag modes plus a rigid pitch and a torsion mode. The hingeless-rotor blade was modeled as a cantilevered beam. The lag damper was modeled using modal damping with the damping levels determined from the blade motion of each mode at the damper attachments. After the initial correlation effort, CAMRAD/JA was modified to incorporate a nonlinear lag-damper model. Effects of the nonlinear lag-damper and various modal-damping levels are examined in the paper. The control-system stiffness was chosen to match the first torsion mode obtained from WHL's J134 mode prediction program (Ref. 19). The blade natural frequencies in vacuo are calculated by J134 and CAMRAD/JA as shown in Fig. 8. Measured frequency data, however, are not available for correlation.

CAMRAD/JA has an option to calculate the blade bending moments using either a curvature method or an integrated force method. The curvature method calculates the structural bending moments from the curvature of the blade modal response; the integrated force method calculates the bending moments by integrating the differences between the inertial and aerodynamic loads. Both methods, however, have their deficiencies. The curvature method is not accurate near a rapid change in stiffness distribution or concentrated load; the integrated force method is sensitive to small errors in the inertial and aerodynamic loads because of small differences of large loads. Results from both methods are compared and discussed.

The aerodynamic model in CAMRAD/JA is based on a second-order, lifting-line theory and uses two-dimensional airfoil characteristics. The airfoil characteristics of the Lynx rotor blade were obtained from small-scale wind tunnel tests. The test data were limited to a Mach number of 0.8 with an angle of attack range of -2 deg to 13.5 deg. The airfoil characteristics of a NACA 0012 were assumed in the analysis for conditions beyond these ranges. Figure 9 presents the airfoil data boundary and the calculated blade angle of attack (α) as a function of Mach number. For Flight 503 condition H, the calculated results reveal that α can be as high as 25 deg, whereas the airfoil data are limited to at most 13.5 deg. The blade aerodynamics were modeled by using 19 aerodynamic segments extending from r/R=0.283 to the tip. CAMRAD/JA has the option of using either a prescribed- or a free-wake model with nonuniform inflow.

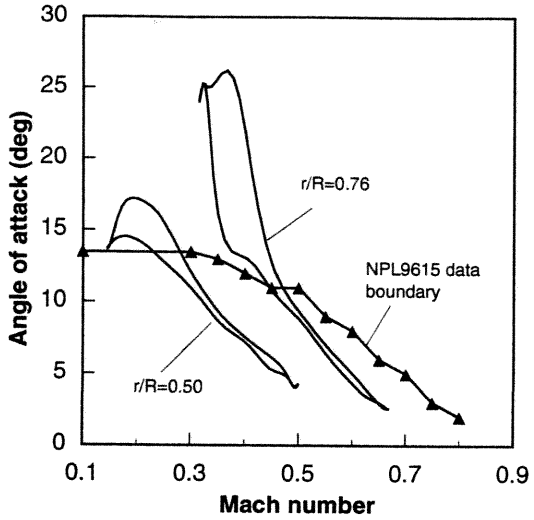

Figure 9. CAMRAD/JA calculation of the blade section angle of attack for Flight 503 condition H.

The prescribed-wake model has a prescribed tip-vortex trajectory. The free-wake model is based on Scully's free wake geometry. The dynamic-stall model used in the analysis calculates an effective α with a correction proportional to $\sqrt{|\alpha|}$ before the evaluation of blade sectional lift, drag, and moment coefficients (Refs. 20-22).

Approach

The low-load case (Flight 487) and the high-load case (Flight 503) were selected for correlation with flight data (see Fig. 5). Table 2 lists the corresponding advance ratios for these flight conditions. The calculated rotor performance and control inputs were compared with flight data for all conditions in Flights 487 and 503. The calculated bending moments, pitch-link load, and lag-damper load, however, were compared only with data from conditions B and H in Flight 487, and conditions A and H in Flight 503.

Table 2. Flight conditions selected for correlation study.

	Advance ratio	
Condition	F487 (C_w/σ=0.07)	F503 (C_w/σ=0.11)
A	—	0.164
B	0.150	—
C	0.199	0.205
D	0.245	—
E	—	0.231
F	0.333	0.243
G	—	0.257
H	0.370	0.270

A baseline model was developed in CAMRAD/JA for the flight conditions mentioned above. Modeling parameters were then varied to examine the sensitivity and the accuracy of the load calculations. These parameters include the lag-damper model, the wake model, and the stall model. In addition, the curvature and integrated force methods were used to calculate the structural loads; effects of rotor trim options on the correlation were also examined. Influence of the fuselage on blade loads was studied using the R150 analysis and compared with flight data.

Results

Rotor Performance and Control Inputs

Figure 10 compares the calculated normalized power of the main rotor with the power obtained in flight as measured from the mean rotor-shaft torque and the rotational speed. Although the free-flight trim was used in CAMRAD/JA performance correlation, results from using the hub-moment trim are about the same. For Flight conditions 503, both CAMRAD/JA and R150 calculations exhibit the correct trend of power requirement as a function of advance ratio . However, the power is overestimated by CAMRAD/JA at moderate speeds and underestimated at high speeds. The underestimation may be attributed to insufficient airfoil data as shown in Fig. 9 and an inadequate dynamic-stall model. The R150 analysis consistently underestimates the required power for this flight condition. The poor power correlation may be associated with an insufficient treatment of yawed-flow effects on drag in separated flow conditions. For Flight conditions 487 both models

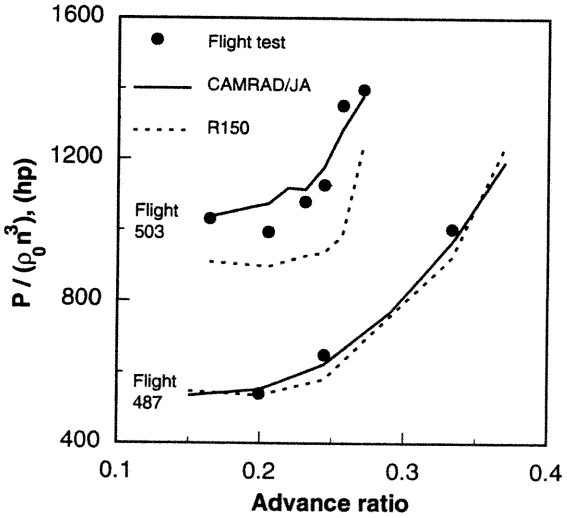

Figure 10. Normalized main-rotor power of Flight conditions 503 and 487.

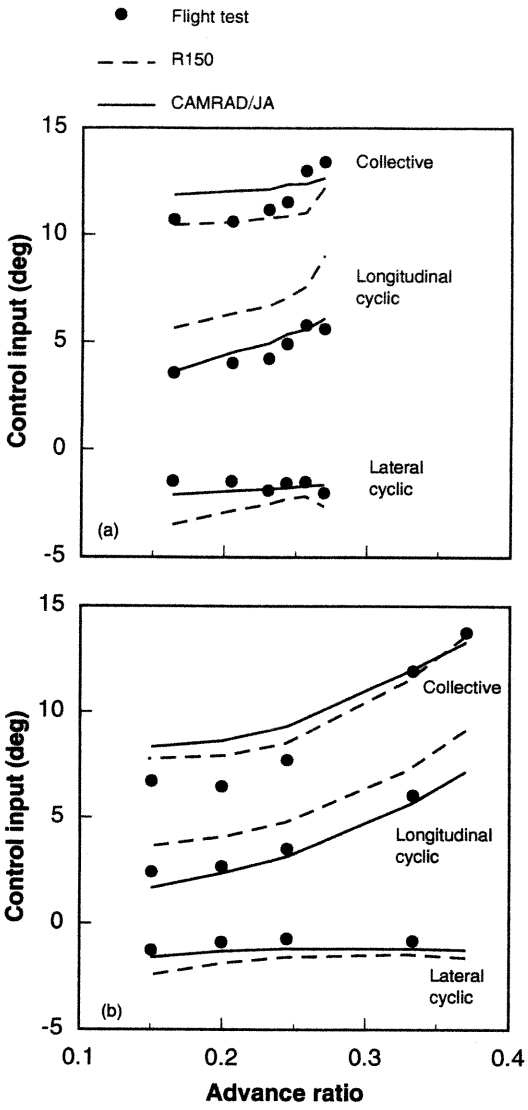

Figure 11. Comparison of calculated control inputs with flight-test data; (a) Flight 503, (b) Flight 487.

calculate the required power accurately.

The calculated control inputs are compared with flight data in Fig. 11. The cyclic-pitch data are extracted from the first harmonic of the feathering angle measurement. CAMRAD/JA control inputs are obtained from the free-flight trim calculations. For Flight conditions 503, CAMRAD/JA calculations of the collective pitch are overestimated by up to 1.5 deg at low speeds and underestimated at high speeds (Fig. 11 (a)). Calculations of the collective pitch are consistent with the power calculations in Fig. 10. R150 calculations of the collective pitch match the data at low speeds but not at high speeds. The cyclic-pitch estimations from CAMRAD/JA compare reasonably well with flight data as shown in Fig. 11 (a). The longitudinal- and lateral-

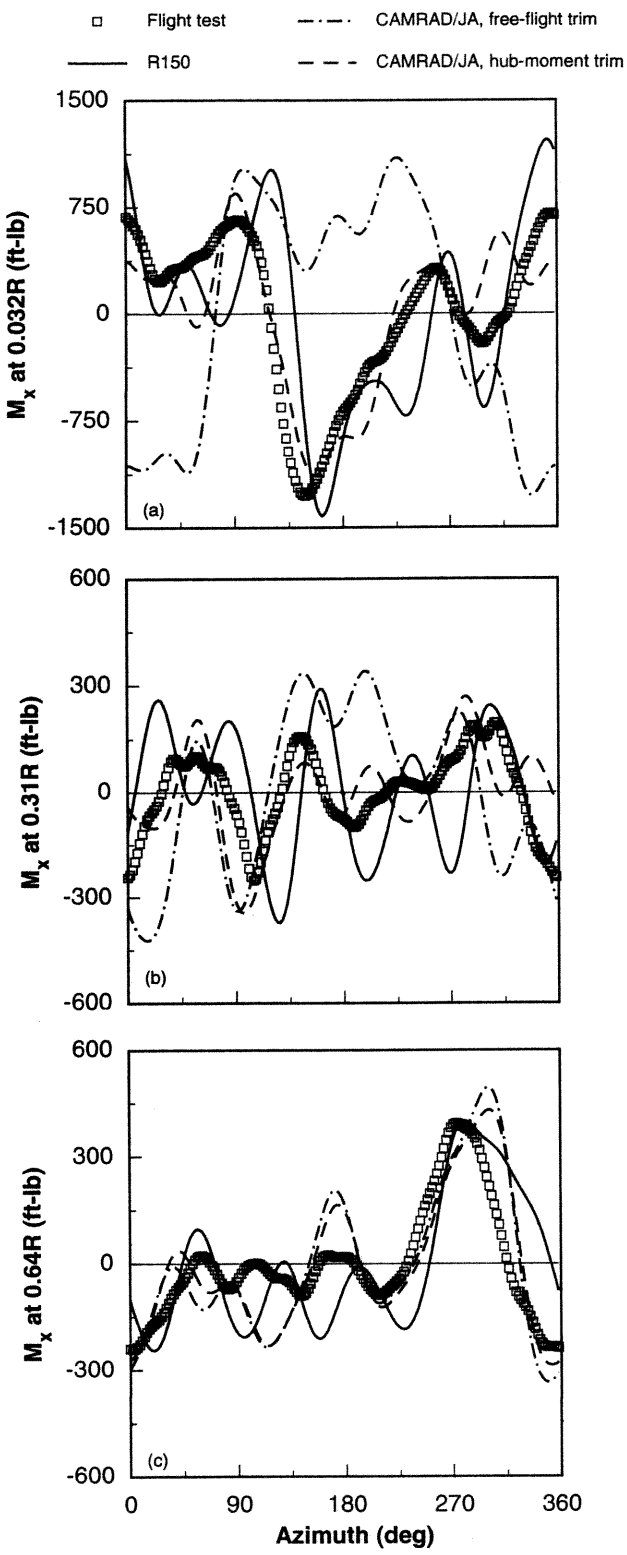

Figure 12. Effect of trim option on flatwise bending moments for Flight 503 condition A; (a) r/R=0.032, (b) r/R=0.31, and (c) r/R=0.64.

cyclic pitches calculated by R150 differ from the flight data by as much as 2 deg. For Flight conditions 487, the collective pitches calculated by each analysis are overestimated at low speeds but are well-correlated at high speeds (Fig. 11 (b)). CAMRAD/JA calculations of the cyclic pitches match the data well. R150 shows a difference of up to 2 deg in the longitudinal and 1.5 deg in the lateral cyclic calculations from the data. If the free-flight trim option is used in the R150 analysis, the resulting cyclic pitches are similar to CAMRAD/JA results. However, correlation of the rotor once-per-revolution (1/rev) flatwise bending moment would deteriorate, as similar to CAMRAD/JA results shown in next section.

Flight 503 condition A — high-thrust, low-speed flight (C_W/σ=0.11, μ=0.164)

The effects of free-flight trim and hub-moment trim on blade bending moments are presented in Figs. 12 and 13 for three representative radial stations. Although CAMRAD/JA calculations for the cyclic pitches correlate well with flight data using free-flight trim (Fig. 11 (a)), calculation of the flatwise bending moment near the hub is poor (Fig. 12 (a)). The poor correlation indicates that the calculated pitching moment at the hub is not accurate, perhaps because of errors in the fuselage and tail aerodynamic data. The hub pitching moment influences the rotor shaft angle and determines the tip-path-plane angle relative to the rotor shaft, which in turn determines the blade flatwise bending moment at 1/rev. Also, the poor correlation may be caused by an incorrect assumption of using a nominal center-of-gravity (c.g.) position for all flight conditions. When the free-flight trim is used in the R150 analysis, the resulting flatwise bending moment near the hub has a similar waveform (not shown) as the CAMRAD/JA result in Fig. 12 (a). By trimming the rotor to the measured 1/rev flatwise bending moment near the hub, the CAMRAD/JA flatwise-moment correlation is improved; R150 results correlate reasonably well with flight data. Using this trim option, however, gives poor correlation of the cyclic pitches with flight data.

At the 31% radial station, the hub-moment trim results of CAMRAD/JA correlate reasonably well with flight data while R150 calculations overestimate the magnitude (Fig. 12 (b)). A harmonic analysis reveals that R150 overestimates the 5th harmonic, possibly because of the near-wake excitation; also the proximity of the third flap mode to the 5/rev may amplify the 5th harmonic. At the outboard station, the differences between flatwise moments calculated using two CAMRAD/JA trim options are small (Fig. 12 (c)). Both CAMRAD/JA and R150 results compare well with the data in trend and in magnitude, especially on the retreating side of the rotor.

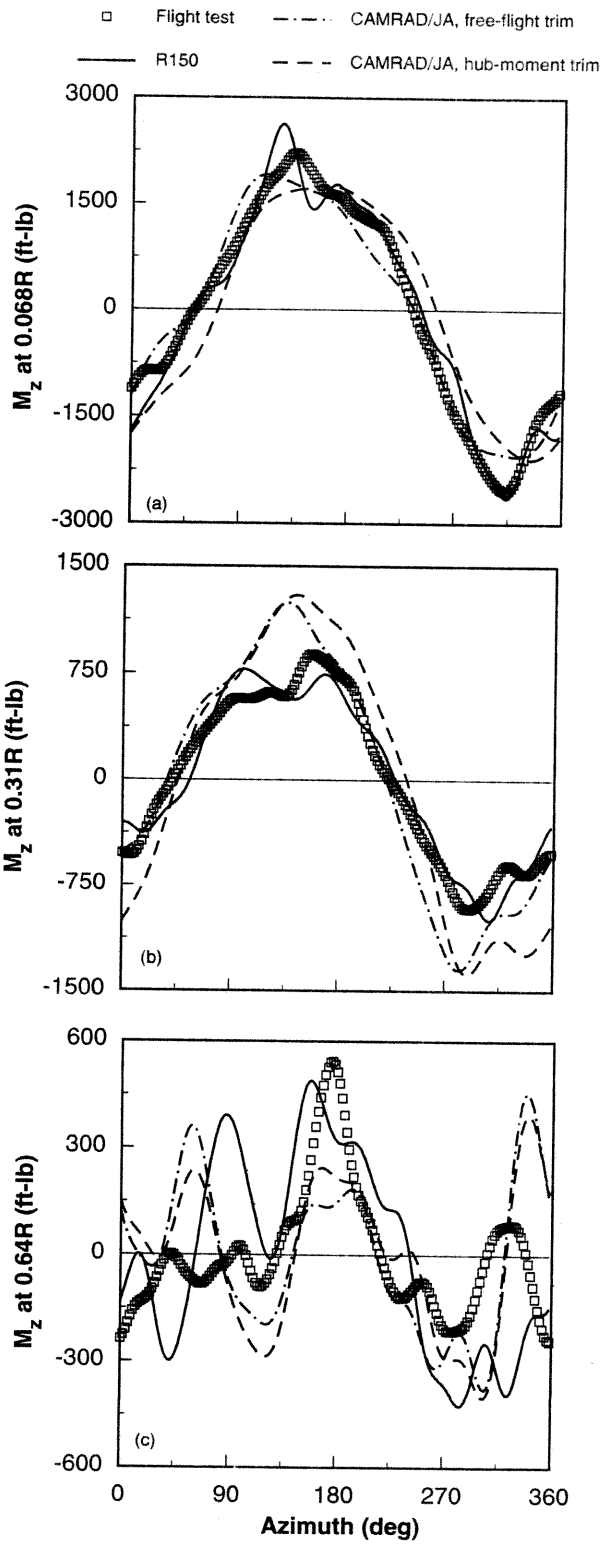

Figure 13. Effect of trim option on edgewise bending moments for Flight 503 condition A; (a) r/R=0.068, (b) r/R=0.31, and (c) r/R=0.64.

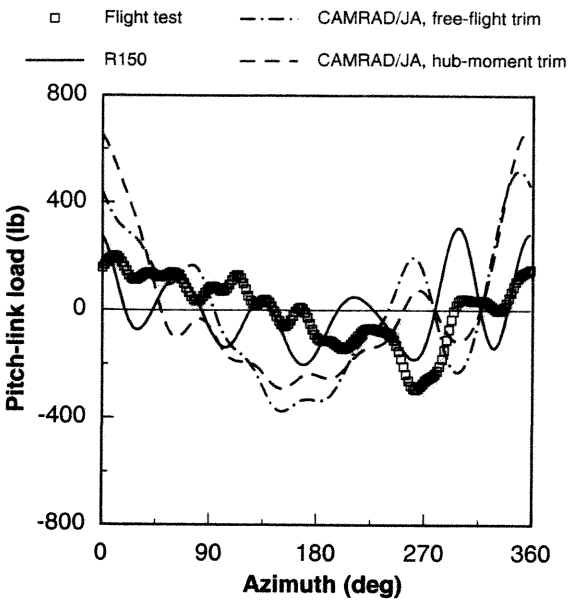

Figure 14. Effect of trim option on pitch-link load for Flight 503 condition A.

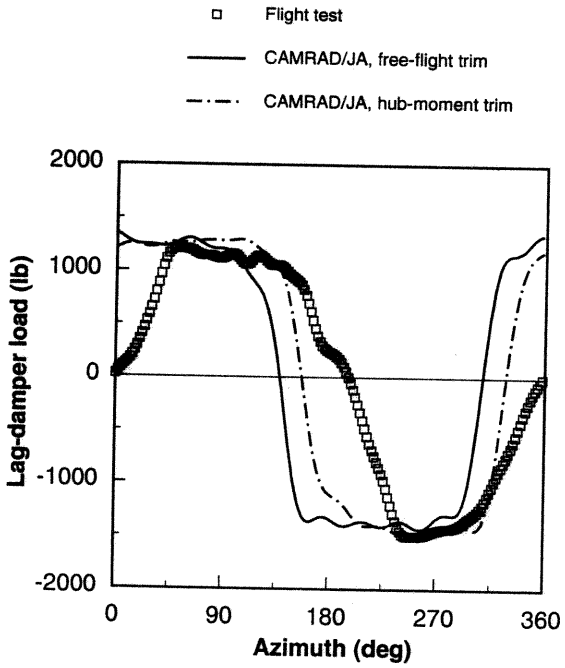

Figure 15. Effect of trim option on lag-damper load for Flight 503 condition A.

The trim option in CAMRAD/JA shows little effect on the edgewise bending moments along the blade (Fig. 13). CAMRAD/JA and R150 calculations of the edgewise bending moment near the hub compare very well with the data (Fig. 13 (a)). At the 31% radial station, the R150 results agree very well with flight data while CAMRAD/JA overestimates the magnitude. At the 64% radial station, the correlation is fair for both the CAMRAD/JA and R150 analyses (Fig. 13 (c)).

Figures 14 and 15 show the calculated pitch-link load and lag-damper load, respectively. Although R150 calculations exhibit the trend of the pitch-link load data, the details of the waveform are not captured. CAMRAD/JA calculation of the pitch-link load compares poorly with flight data. In Fig. 15, the CAMRAD/JA result from the hub-moment trim solution correlates better with the lag-damper load data than the free-flight result.

The effects of CAMRAD/JA lag-damper modeling

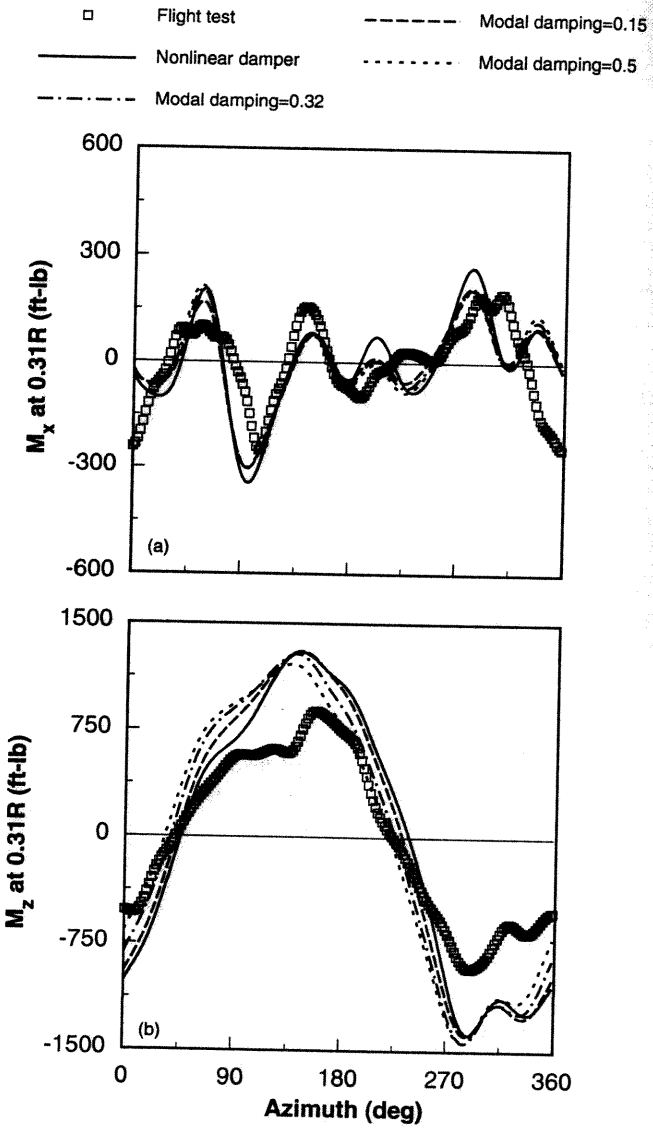

Figure 16. Effect of CAMRAD/JA lag-damper modeling on bending moments at r/R=0.31 using curvature method for Flight 503 condition A; (a) flatwise moment, (b) edgewise moment.

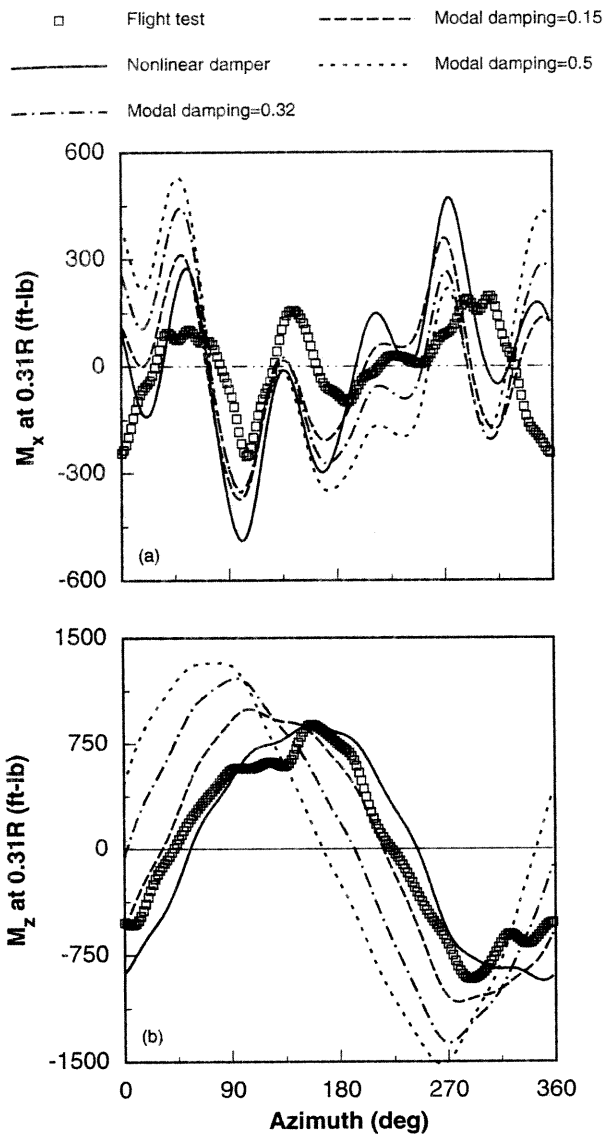

Figure 17. Effect of CAMRAD/JA lag-damper modeling on bending moments at r/R=0.31 using integrated-force method for Flight 503 condition A; (a) flatwise moment, (b) edgewise moment.

on blade bending moments are shown in Fig. 16. Since R150 has a built-in nonlinear lag-damper model, variation of the lag-damper modeling is only applicable to CAMRAD/JA. Little effect on the flatwise and edgewise bending moments at the 31% radial station is observed even with modal damping of the fundamental lag mode varied from 0.15 to 0.5; results are similar to the nonlinear-damper results.

As discussed earlier, CAMRAD/JA can calculate blade bending moments using an integrated force method. The result of varying the modal-damping levels on blade loads using the integrated force method is very different compared to the curvature method (compare Figs. 16 and 17). Using the nonlinear lag-damper model, the flatwise bending moment at the 31% radial station is overestimated (Fig. 17 (a)) but the edgewise moment closely matches the data (Fig. 17 (b)). The overestimation in the flatwise moment is caused by small errors in the inertial and aerodynamic moment calculations. Although not shown, the edgewise moment near the tip region is more accurate when calculated by using the integrated force method than the curvature method. However, the overall results from the curvature method correlate better with data than the integrated-force results. Hence, the curvature method is used for subsequent CAMRAD/JA calculations presented in this paper.

Flight 503 condition H — high-thrust, high-speed flight (C_W/σ=0.11, μ=0.27)

At high thrust and high forward speed, the retreating side of the rotor encounters severe stall. For these conditions, an unsteady aerodynamic stall model is usually recommended for rotor-loads correlation (Ref. 23). The stall models of CAMRAD/JA are evaluated for this flight . Since CAMRAD/JA was unable to obtain a steady-state solution using the hub-moment trim, the free-flight trim is used for this flight condition.

Figure 18 compares the flatwise bending moment calculations for three radial stations using the R150 analysis and CAMRAD/JA's static and dynamic stall models. The flatwise bending moments calculated by CAMRAD/JA compare reasonably well with flight data. Although the dynamic-stall model results contain more harmonic content, no qualitative improvement is observed compared to the static-stall model results. Near 180 deg azimuth, the bending moment at the 3.2% radial station is underestimated by CAMRAD/JA and overestimated by R150 (Fig. 18 (a)). The CAMRAD/JA underestimation results from an incorrect trim angle of the tip-path-plane relative to the rotor shaft. The R150 result reflects the higher harmonic waveform, especially the 3/rev which is the primary source of the aircraft vibration. The magnitude and trend of the flatwise bending moment data are captured by R150 and CAMRAD/JA calculations at the 31% and 64% radial stations (Figs. 18 (b) and (c)).

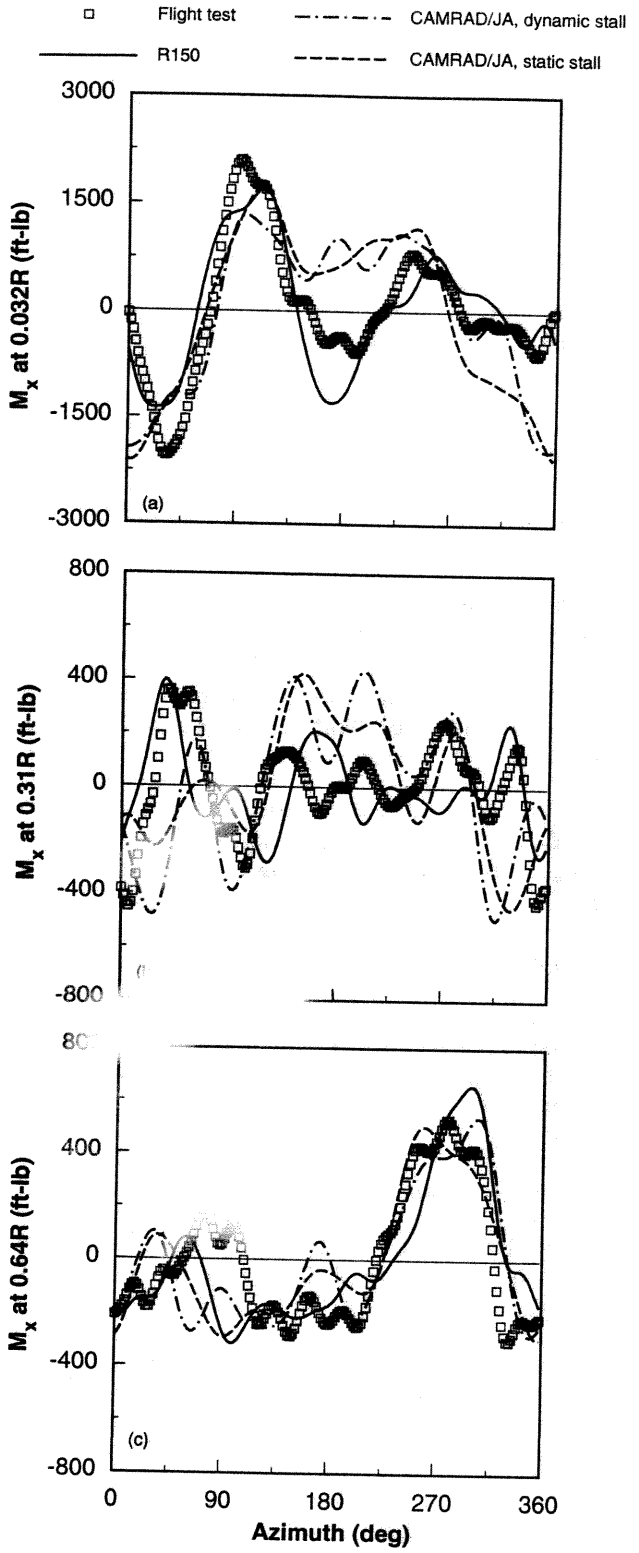

Figure 18. Effect of stall model on flatwise bending moments for Flight 503 condition H. (a) r/R=0.032, (b) r/R=0.31, and (c) r/R=0.64.

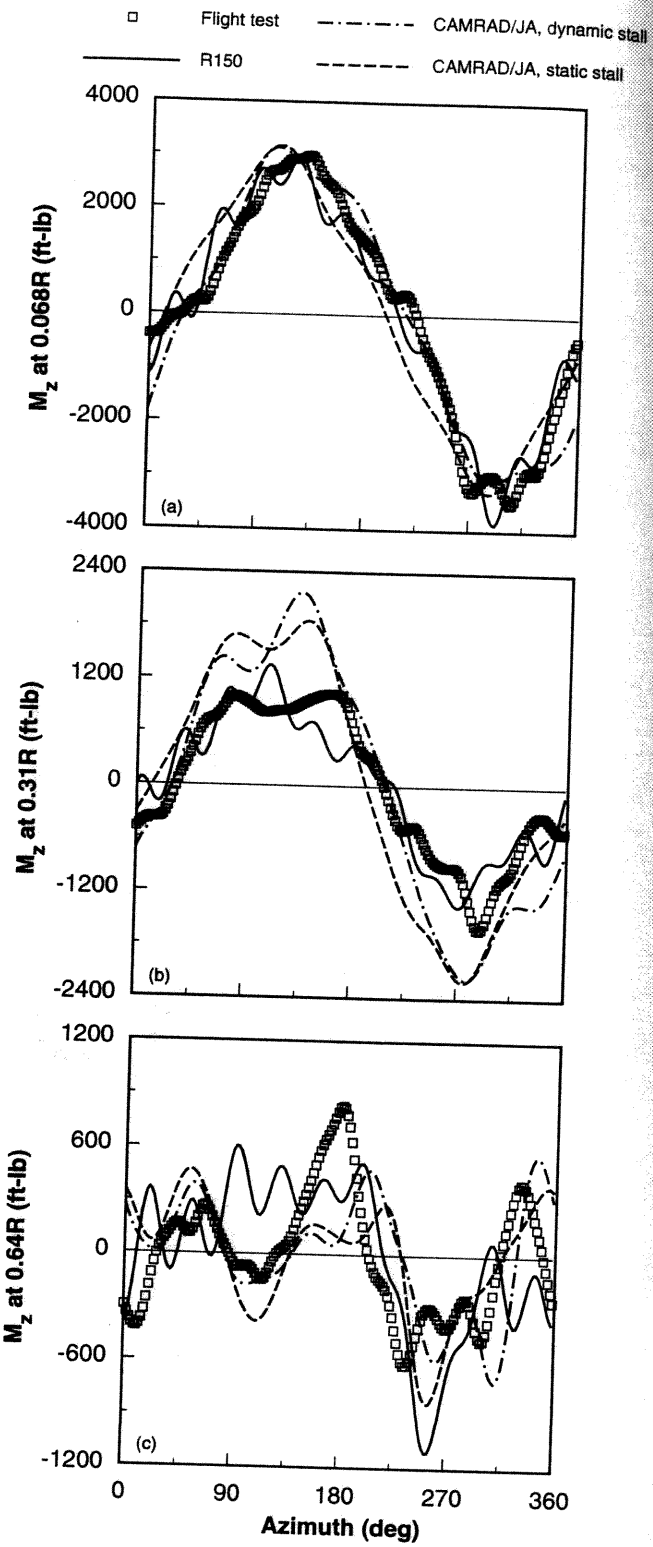

Figure 19. Effect of stall model on edgewise bending moments for Flight 503 condition H. (a) r/R=0.068, (b) r/R=0.31, and (c) r/R=0.64.

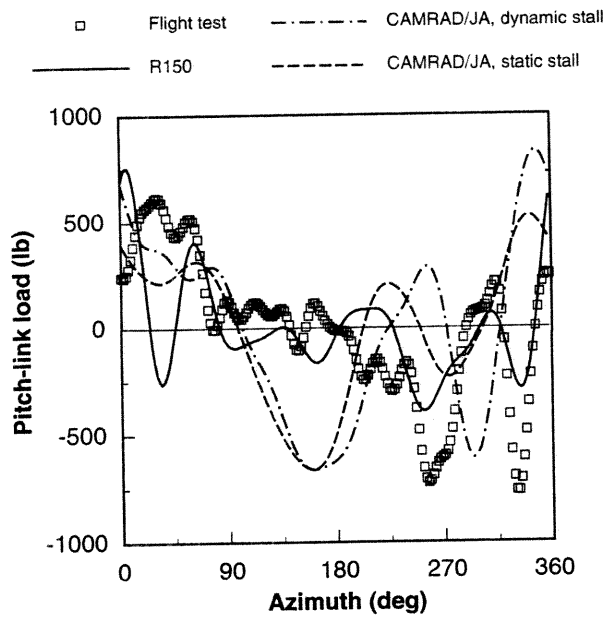

Figure 20. Effect of stall model on pitch-link load for Flight 503 condition H.

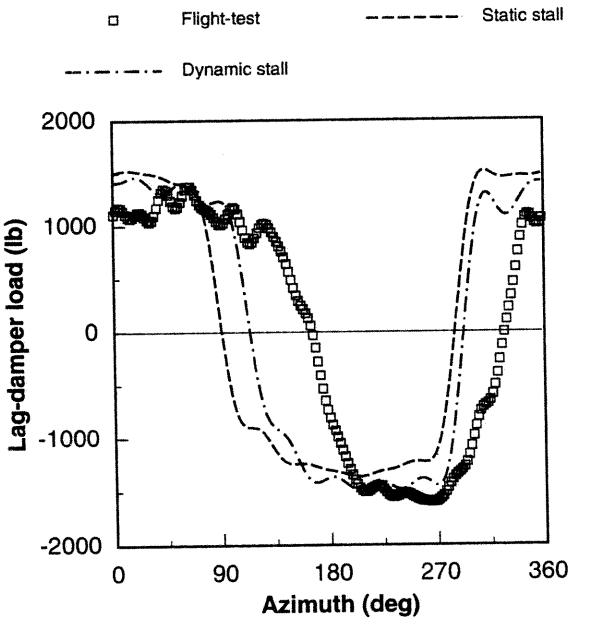

Figure 21. Effect of CAMRAD/JA's stall model on lag-damper load for Flight 503 condition H.

CAMRAD/JA and R150 results correlate very well with the edgewise bending moment data at the 6.8% radial station (Fig. 19 (a)). At the 31% radial station, the CAMRAD/JA calculation overestimates the data (Fig. 19 (b)). The presence of higher harmonic content of the flight data appears near the retreating side of the rotor. The 10/rev harmonic presented in the R150 results reflects an overestimation of the response of the third lag mode compared to the flight data. At the 64% radial station, comparisons of the results from both analytical codes with the data are fair. In general, the dynamic-stall model shows slight improvement in the bending moment correlations over the static-stall model.

No improvement in pitch-link load correlation is gained by using the dynamic-stall model in CAMRAD/JA (Fig. 20). R150 captures the general trend of the waveform, especially the phasing of the initial pitch-down excursion near 270 deg azimuth, which is caused by blade stall, and the subsequent rebound. The consequence of the pitch-up response is to drive the blade further into another stall, which results in a second larger pitch-down response near 300 deg azimuth. R150 correctly models the phasing of this second event, although the predicted control load reversal continues incorrectly on the advancing side. Additionally, a harmonic analysis reveals the presence of very high frequency content in the flight-test data—the magnitude of the 10th harmonic is 25% of the first harmonic. However, the frequency content for R150 and CAMRAD/JA results diminish at the 9th and 7th harmonics, respectively. Although an attempt was made to introduce additional blade modes (nine coupled flap and lag modes plus three torsion modes) with 16 harmonics in the CAMRAD/JA calculation, no improvement was gained. The dynamic-stall model results from CAMRAD/JA, however, correlate better with the lag-damper load data than the static-stall model results (Fig. 21).

Flight 487 condition B — low-thrust, low-speed flight (C_W/σ=0.07, μ=0.15)

At low forward speed, the rotor wake strongly influences the rotor aerodynamics. A detailed wake geometry is necessary to predict the aeroelastic behavior of the rotor blade (Ref. 24). Figures 22 and 23 compare the wake-model effects on flatwise and edgewise bending moments using the hub-moment trim in CAMRAD/JA. With a uniform-inflow model, CAMRAD/JA is unable to capture the higher harmonic content of the flatwise moment data shown in Fig. 22. Using a prescribed-wake model improves the correlation, but results from a free-wake model show the best correlation with flight data. Surprisingly, at the 6.8% radial station, the uniform-inflow results show better correlation with edgewise bending-moment data than the prescribed- and the free-wake results (Fig. 23 (a)). Further outboard from the hub, the free-wake results correlate better with flight data than the prescribed-wake model (Fig. 23 (b)). At the 64% radial station, CAMRAD/JA calculation of the edgewise moment compares poorly with data (Fig. 23 (c)).

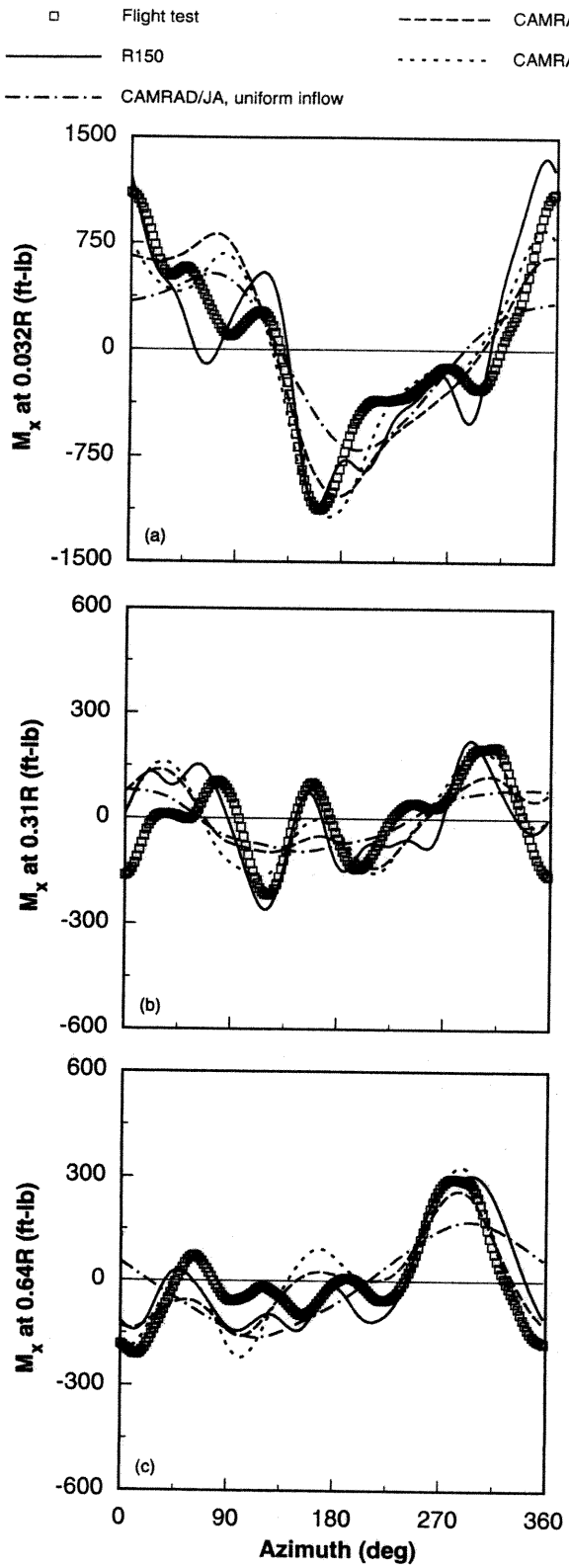

Figure 22. Effect of wake model on flatwise bending moments for Flight 487 condition B; (a) r/R=0.032, (b) r/R=0.31, and (c) r/R=0.64.

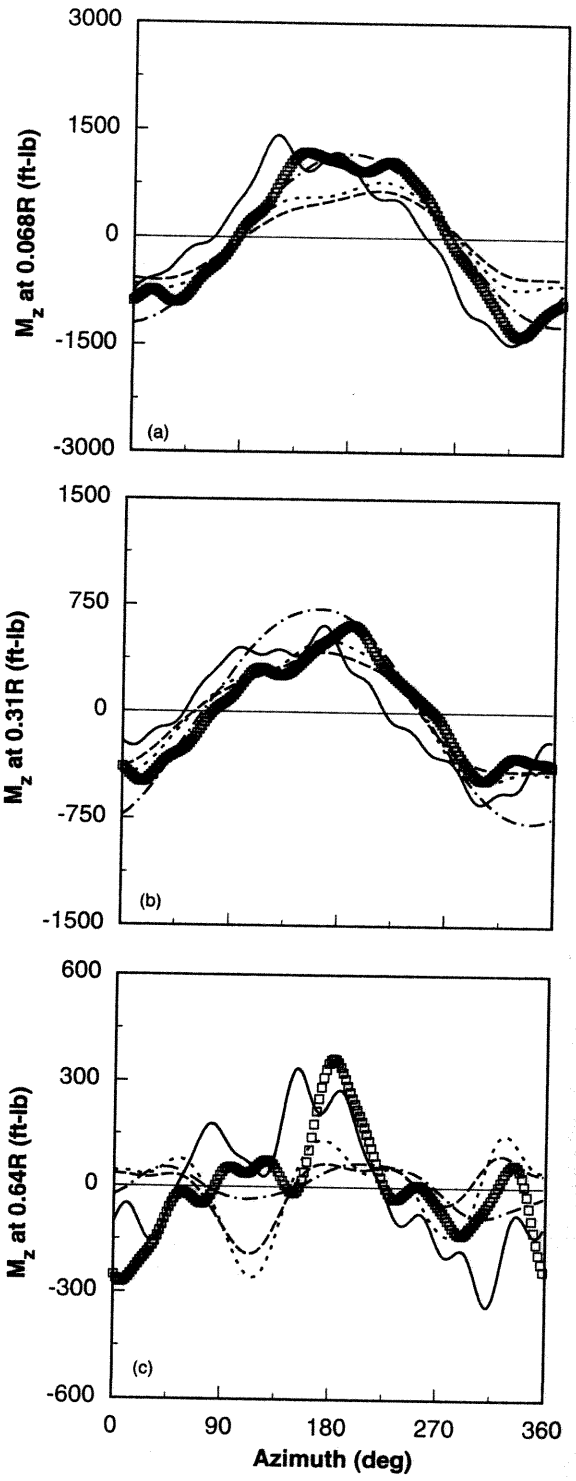

Figure 23. Effect of wake model on edgewise bending moments for Flight 487 condition B; (a) r/R=0.068, (b) r/R=0.31, and (c) r/R=0.64.

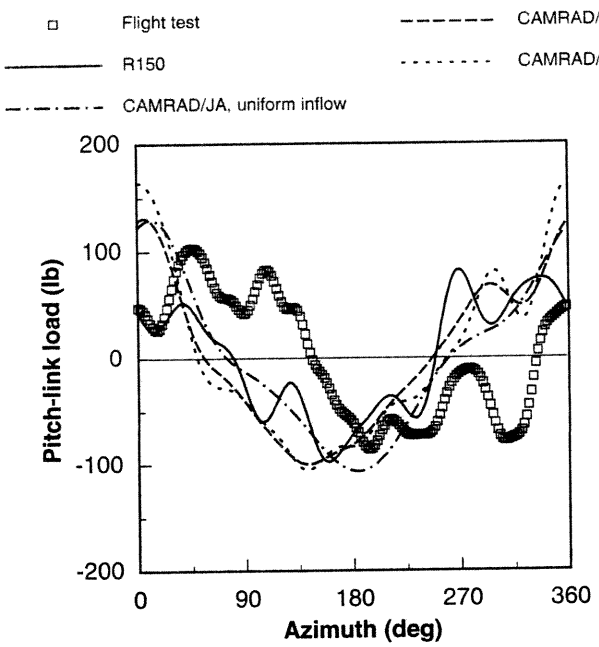

Figure 24. Effect of wake model on pitch-link load for Flight 487 condition B.

The flatwise bending moments are well-estimated by R150's vortex-ring model (Fig. 22). The R150 flatwise moments match the data better at the low-thrust condition than at the high-thrust condition (compare Figs. 12 and 22). The edgewise moments, however, are better correlated with data at the high-thrust condition than at the low-thrust condition (compare Figs. 13 and 23).

Both CAMRAD/JA and R150 results exhibit the trend of the pitch-link load data but not the waveform (Fig. 24). The prescribed- and free-wake results offer no improvement over the uniform inflow results. Near 270 deg azimuth, the R150 result reflects the pitch-link reversal load quite well.

Flight 487 condition H — low-thrust, high-speed flight (C_W/σ=0.07, μ=0.37)

For this flight condition, the fuselage effects on R150 bending-moment results are presented in Figs. 25 and 26. Including the fuselage aerodynamic model improves the flatwise bending moment calculation at the 3.2% and 31% radial stations, especially on the retreating side of the rotor (Fig. 25 (a) and (b)). At the outboard station, the fuselage effect is less significant (Fig. 25 (c)). R150 correlation of the edgewise moment near the hub is only fair because the second harmonic is underestimated (Fig. 26 (a)). Further outboard from the hub, the edgewise moment calculations are poor (Fig. 26 (b) and (c)). The fuselage effect is most noticeable near 180 deg azimuth for the 31% and 64% radial stations, where flow over the helicopter nose creates an upwash into the rotor plane.

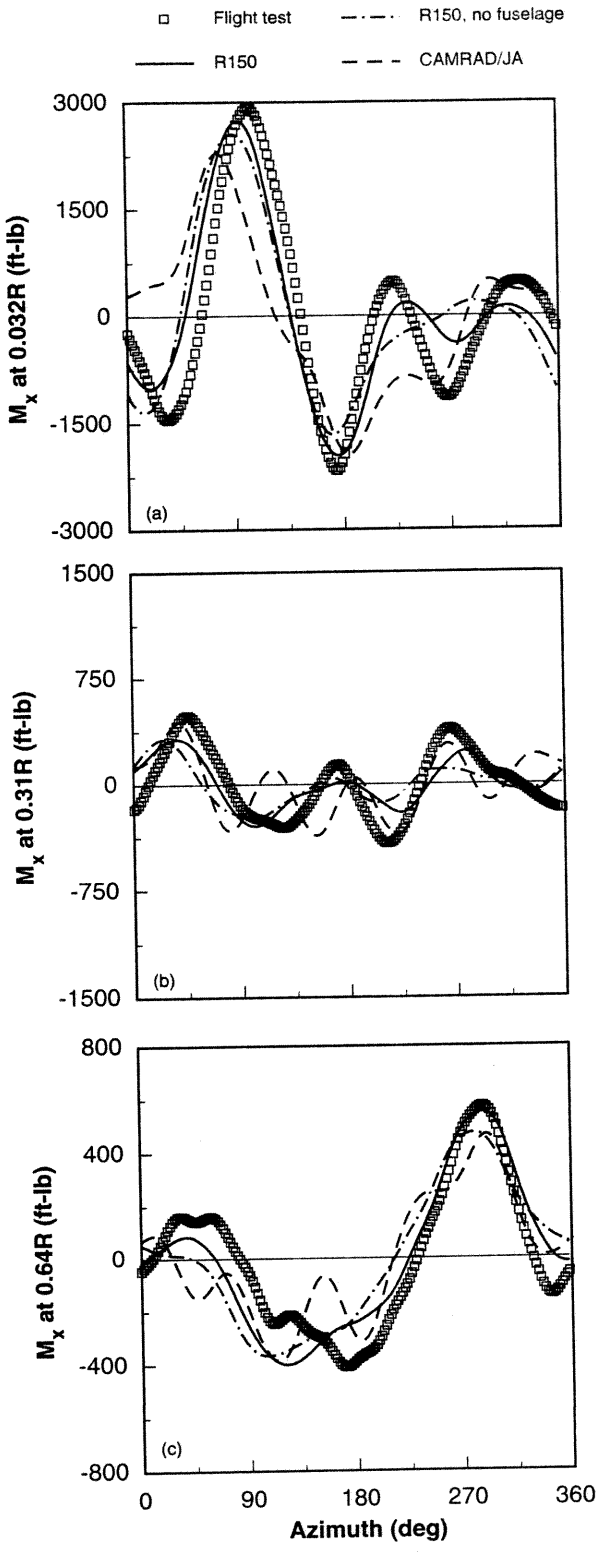

Figure 25. Fuselage effect on flatwise bending moments for Flight 487 condition H; (a) r/R=0.032, (b) r/R=0.31, and (c) r/R=0.64.

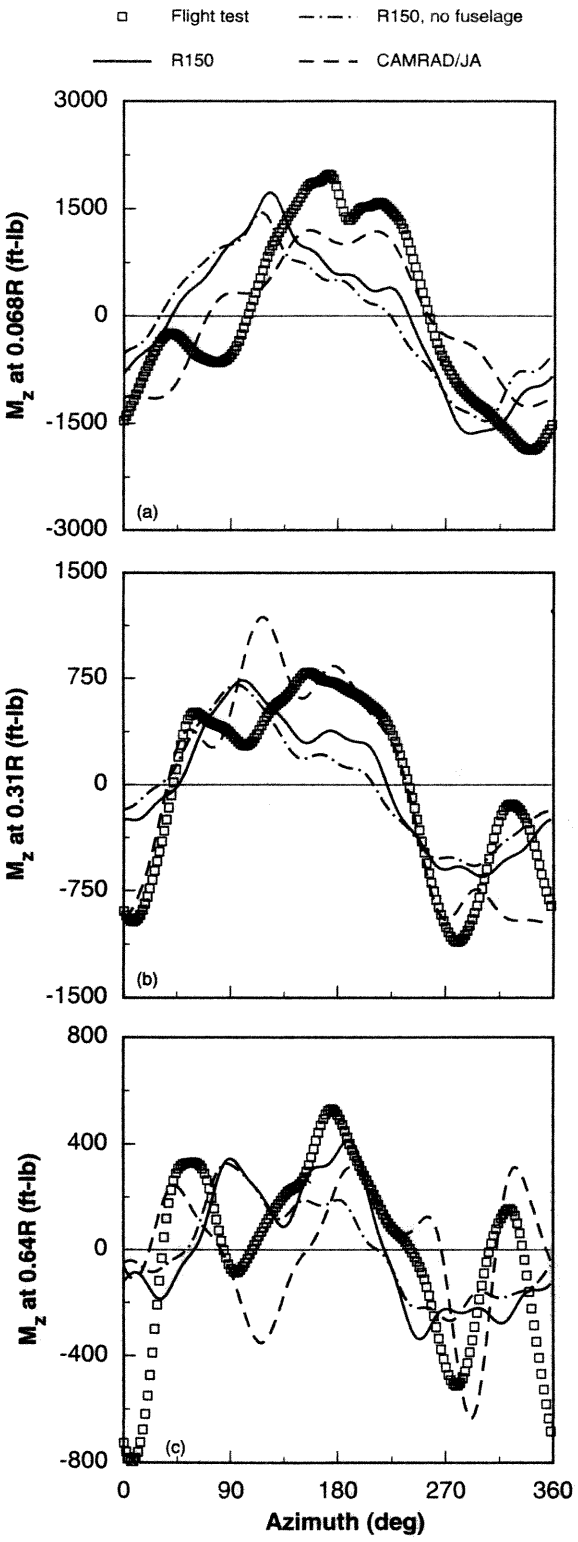

Figure 26. Fuselage effect on edgewise bending moments for Flight 487 condition H; (a) r/R=0.068, (b) r/R=0.31, and (c) r/R=0.64.

CAMRAD/JA results are calculated using the hub-moment trim for this flight condition. The flatwise moment correlations are fair at the 3.2% and 31% radial stations but improve at the 64% radial station (Fig. 25). The edgewise moment correlations are good near the hub and at the inboard station (Fig. 26 (a) and (b)). At the 64% radial station, the trend of the data is well captured by CAMRAD/JA, especially the higher harmonic reversal near 270 deg azimuth.

Finally, the trend of the pitch-link load data is reasonably matched by results from both analyses but details of the waveform are not (Fig. 27).

Conclusions

Results of the CAMRAD/JA and R150 analyses were compared with the Lynx-XZ170 data for flight conditions below and above the rotor stall boundary. The following conclusions are based on the results from the correlation study.

Performance, control inputs, and blade frequencies

1) CAMRAD/JA calculations of rotor performance for high- and low-thrust flight conditions match the flight data reasonably well. R150 calculations underestimate the rotor power for high-thrust flight conditions and match the power for low-thrust flight conditions.

2) Results from the free-flight trim show reasonably

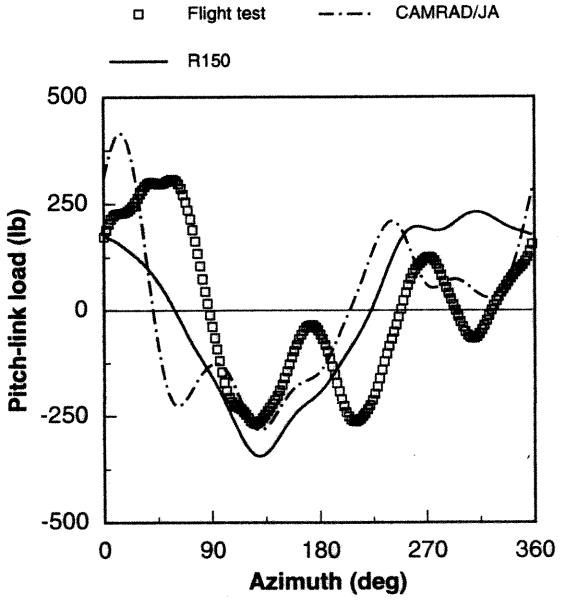

Figure 27. Pitch-link load for Flight 487 condition H.

good correlation of the cyclic pitches but poor correlation of the flatwise bending moments (especially near the hub) with flight data. On the other hand, results from the hub-moment trim provide poor correlation of the cyclic pitches but good correlation of the flatwise moments. A trade off exists between the flatwise moment and cyclic-pitch correlations in both the CAMRAD/JA and R150 analyses.

3) CAMRAD/JA and J134 calculations of the blade natural frequencies in vacuo are consistent with each other.

Rotor loads

General remarks

1) Near the hub, the free-flight trim calculation of flatwise bending moment, especially the 1/rev harmonic, is overestimated. Using the hub-moment trim remarkably improves the correlation. An accurate free-flight trim model is necessary to calculate the blade loads.

2) The modal-damping model in CAMRAD/JA is adequate to simulate the lag damper. Loads calculated by the curvature method are less sensitive to variations in damping levels than the integrated-force results.

3) In general, the bending-moment results from CAMRAD/JA's curvature method are more accurate than the integrated-force results (except the edgewise bending moment near the tip region).

4) Although the general trends of the pitch-link load data are reasonably matched by both R150 and CAMRAD/JA results, the waveform details are not. The magnitudes are consistently overestimated by CAMRAD/JA, possibly because the actual geometry of the hub (pitch link, pitch horn, and swashplate) is not modeled since the pitch/torsion dynamics are approximated.

High-thrust, low-speed flight

1) Using the hub-moment trim option, CAMRAD/JA correlations of the flatwise bending moment are very good near the hub and reasonably good at the inboard and outboard stations. R150 results correlate very well near the hub and at the outboard station but fairly at the inboard station.

2) CAMRAD/JA calculations (using either trim option) of the edgewise bending moments compare very well near the hub and reasonably well at the inboard station. R150 correlations are very good near the hub and at the inboard station. At the outboard station, correlations from both analyses are fair.

3) Except for a phase difference, the lag-damper load is well-estimated by CAMRAD/JA using hub-moment trim.

High-thrust, high-speed flight

1) Bending-moment correlations (using free-flight trim) are improved slightly using CAMRAD/JA's dynamic-stall model. However, the lag-damper load correlation improves noticeably using the dynamic-stall model instead of the static-stall model.

2) A fair comparison is achieved between the data and CAMRAD/JA calculations of flatwise bending moments near the hub and at the inboard station; the comparison is better at the outboard station. R150 correlations are good near the hub and at the outboard station but only fair at the inboard station.

3) The edgewise bending moments calculated by both analyses compare well with the data near the hub; the comparison is fair at the outboard station. At the inboard station, R150 results correlate very well with flight data while CAMRAD/JA results overestimate the data.

Low-thrust, low-speed flight

1) In general, bending moment calculations using CAMRAD/JA's free-wake model with nonuniform inflow correlate better with flight data than the uniform inflow and the prescribed-wake model results

2) CAMRAD/JA correlations of the flatwise bending moments are very good near the hub and reasonably good at the inboard and outboard stations. R150 correlations are very good along the blade span.

3) The edgewise moment data are well-matched by both CAMRAD/JA and R150 results near the hub and at the inboard station. At the outboard stations, correlations are fair for both analyses.

Low-thrust, high-speed flight

1) Including the fuselage model noticeably improves the R150 flatwise bending moment correlation at the inboard station.

2) R150 correlation of the flatwise bending moments is very good along the blade span. CAMRAD/JA results compare reasonably well near the hub and at the

inboard station; the comparison improves at the outboard station.

3) R150 and CAMRAD/JA edgewise moments correlate better with flight data at the inboard station than at the outboard station, although CAMRAD/JA results capture the data trend well at the outboard station.

Recommendations

The following are recommended for improvement in future analytical developments and tests.

Test results and data reduction

1) Obtain the c.g. position of the aircraft in flight and use it in the aircraft trim analysis.

2) Acquire the blade aerodynamic characteristics with a full-scale airfoil and obtain a wider range of α and Mach number.

3) Obtain experimental data of the rotating blade frequencies to substantiate the accuracy of the analytical results.

Analytical developments

1) Continue the exploration of the ability to calculate the blade structural loads in extreme operating conditions, including the influences of root load paths (pitch link, control system, and lag damper) and to develop a better dynamic stall model.

2) Conduct an experimental and theoretical investigation of the swept flow effect on aerodynamic characteristics in stall.

3) Improve the free-flight trim model to calculate the hub moment and control inputs accurately.

Acknowledgments

The work reported here was performed under the auspices of HTP-6 of TTCP between the United Kingdom and the United States of America. The authors would like to thank Mr. Robert Hansford of WHL and Dr. William Warmbrodt of NASA Ames who established the joint research program and have made the project possible. The authors would also like to thank Dr. Wayne Johnson of Johnson Aeronautics for his guidance throughout the project.

References

1 Scheiman, J., "A Tabulation of Helicopter Rotor-Blade Differential Pressures, Stresses, and Motions as Measured in Flight," NASA TM X-952, Mar. 1963.

2 Rabbott, J. P. Jr., Lizak, A. A., and Paglino, V. M., "A Presentation of Measured and Calculated Full-Scale Rotor Blade Aerodynamic and Structural Loads," USAAVLABS TR 66-31, Jul. 1966.

3 Beno, E. A., "CH-53A Main Rotor and Stabilizer Vibratory Airloads and Forces," Sikorsky Engineering Report 65593, Jun. 1970.

4 Johnson, W., "Performance and Loads Data From a Wind Tunnel Test of a Full-Scale Rotor with Four Blade Tip Planforms," NASA TM 81229, Sept. 1980.

5 Heffernan, R. and Gaubert, M., "Structural and Aerodynamic Loads and Performance Measurements of an SA 349/2 Helicopter with an Advanced Geometry Rotor," NASA TM 88370, Nov. 1986.

6 Felker, F. F. III, "Performance and Loads Data from a Wind Tunnel Test of a Full-Scale, Coaxial, Hingeless Rotor Helicopter," NASA TM 81329, Nov. 1981.

7 Peterson, R. and Warmbrodt, W., "Hover Test of a Full-Scale Hingeless Helicopter Rotor: Aeroelastic Stability, Performance, and Loads Data," NASA TM 85892, Jan. 1984.

8 Bartsch, E. A., "In-Flight Measurement and Correlation With Theory of Blade Airloads and Response on the XH-51A Compound Helicopter Rotor, Volume I—Measurement and Data Reduction of Airloads and Structural Loads," USAAVLABS TR 68-22A, May 1968.

9 Lau, B., Louie, A., Griffiths, N., and Sotiriou, C., "Performance and Rotor Loads Measurements of the Lynx XZ170 Helicopter with Rectangular Blades," NASA TM 104000, 1993.

10 Johnson, W., "CAMRAD/JA. A Comprehensive Analytical Model of Rotorcraft Aerodynamics and Dynamics, Johnson Aeronautics Version. Volume I: Theory Manual," Johnson Aeronautics, 1988.

11 Hansford, R. E., "A Unified Formulation of Rotor Load Prediction Methods," *Journal of the American Helicopter Society*, Volume 31, (2), Apr. 1986.

12 Beddoes, T. S., "Rotor Performance Program Improvements–Sweep and Tip Relief Effects," Westland Helicopters Limited, Internal Report, Research Memorandum 223, Mar. 1974.

13 Beddoes, T. S., "A Synthesis of Unsteady Aerodynamic Stall Hysteresis," First European Rotorcraft Forum, Southampton, England, Sept. 1975.

14 Beddoes, T. S., "Onset of Leading Edge Separation Effects Under Dynamic Conditions and Low Mach Numbers," American Helicopter Society 34th Annual Forum, Washington D. C., May 1978.

15 Young, C., "Development of the Vortex Ring Wake Model and Its Influence on the Prediction of Rotor Loads," AGARD Conference Proceeding No. 334, May 1982.

16 Howell, D., "A Description of the Modal Analysis Technique for the Analysis of Rotor System Flight Test Records," Westland Helicopters Limited, Internal Report, WG13/DYN/010R, Jun. 28, 1972.

17 Griffiths, N., "Specification for Program ACTRIM (Issue A) Program to Calculate Longitudinal Trim of Aircraft," Westland Helicopters Limited, Internal Report, Dynamic Department Notes, DYN/90/59.

18 Sotiriou, C. P., "WHL-NASA Ames Collaborative Study on Lynx (Metal Blade) Structural Loads (Interim Report)," Westland Helicopters Limited, Internal Report, Dynamic Department Report, DYN/91/23, 1991.

19 King, S., "Blade Equations by Energy Method," Westland Helicopters Limited, Internal Report, GEN/DYN/209N, 1978.

20 Harris, F. D., Tarzanin, F., and Fisher, R., "Rotor High Speed Performance, Theory vs. Test," *Journal of the American Helicopter Society*, Volume 15, (3), Jul. 1970.

21 Tarzanin, F., "Prediction of Control Loads due to Blade Stall," *Journal of the American Helicopter Society*, Volume 17, (2), Apr. 1972.

22 Gormont, R. E., "A Mathematical Model of Unsteady Aerodynamics and Radial Flow for Application to Helicopter Rotors," USAAVLABS TR 72-67, May 1973.

23 Arcidiacono, P. and Sopher, R., "Review of Rotor Loads Prediction Methods," AGARD Conference Proceedings No. 334, May 1982.

24 Yamauchi, G. K., Heffernan, R. M., and Gaubert, M., "Correlation of SA349/2 Helicopter Flight Test Data with a Comprehensive Rotorcraft Model," *Journal of the American Helicopter Society*, Volume 33, (2), Apr. 1988.